
Check for updates

[9], whe
at an incident ion energy $E_i \sim 80$ eV
out the effect of molecular ions on the evaluation of incident ion flux (Γ_i)/fluence (ϕ_i) as well as of E_i, He plasma was selected instead of H or D plasma. The sputtering yield of Cr, Y, was determined from weight loss measurements. Namely, a mass change between before and after plasma exposure was measured with a microbalance at each site. Plasma parameters, including Γ_i, plasma space potential, V_s, electron density, n_e, and electron temperature, T_e, were measured using a reciprocating Langmuir probe in each device. To minimize redeposition of sputtered Cr atoms onto the Cr sample, the plasma exposure was performed at relatively low $\Gamma_i < 1 \times 10^{22}$ m^{-2}s^{-1} and $T_e \sim$ 4–6 eV. The sample temperature, T_s, was measured with a thermocouple attached to the backside of the sample in PISCES-A and PSI-2. In PSI-2, an infrared camera was also used to monitor T_s from the front surface. In NAGDIS-II, a pyrometer was employed to measure T_s. Since enhanced erosion was observed at $T_s > 400$ °C in a dedicated experiment in PISCES-A, T_s was kept below 400 °C in all the experiments. The time evolution of a relative change in the sputtering yield of Cr was monitored with spectroscopic measurements of visible Cr I lines (425.4 nm, 427.4 nm, and 428.9 nm) during plasma exposure. The emission intensity of the Cr I lines was collected in front of the Cr target. To compensate for any changes in the plasma condition and the vacuum window transmission, He I lines (438.8 nm in all the devices and 447.1 nm only in PISCES-A) were also monitored. Note that, as presented below, the combination of Cr I and He I lines is different for each device to avoid using saturated lines. In PSI-2, a quartz microbalance (QMB) was also used as a complement to spectroscopy. Surface morphology of the Cr sample after plasma exposure was observed with a scanning electron microscope (SEM) at each site.

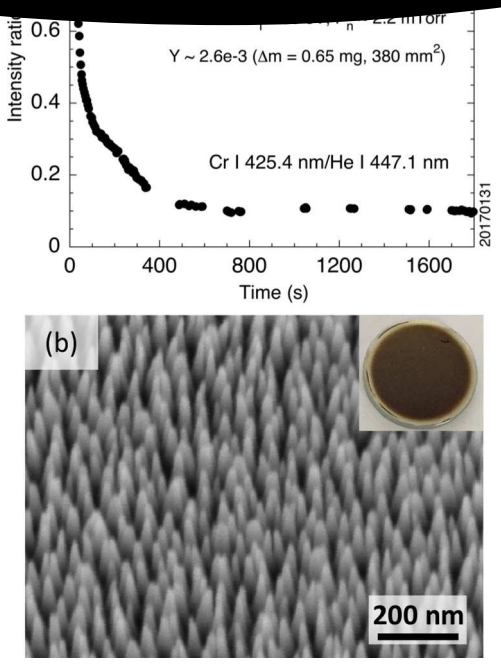

Fig. 1. Typical Cr sputtering experimental result in PISCES-A. (a) Time evolution of the intensity ratio, Cr I 425.4 nm/He I 447.1 nm, measured in front of a Cr sample during He plasma exposure. (b) SEM image of the Cr sample after the He plasma exposure. A photo of the entire Cr sample is shown in the inset.

3. Experimental results

In this section, typical experimental results from each device are summarized.

3.1. PISCES-A

The experiments were first conducted in PISCES-A. A typical time trace of the Cr I 425.4 nm line intensity normalized to the He I 447.1 nm line intensity during He plasma exposure in PISCES-A is plotted in Fig. 1(a). In this experiment, the intensity ratio of ~0.85 at the beginning dropped quickly and reached the saturation level of ~ 0.1 at ~400 s. Correspondingly, the time-integrated measured $Y \sim$ 2.6e-3 is much lower than the theoretical value of ~3.7e-2 [1]. After the plasma exposure, the sample surface appeared dark (see the photo inside Fig. 1(b)), and cone structures well developed on the surface, as shown in Fig. 1(b). In contrast, Ne plasma exposure did not lead to the formation of cone structures, and hence the measured sputtering yield agreed with values from Ref. [1]. These observations are consistent with our previous experiments using other metals [2–4].

3.2. PSI-2

The next experiments were made in PSI-2 to reproduce the observations in PISCES-A. However, results obtained in PSI-2 contradicted those in PISCES-A. Only a slight decrease (~20%) in an intensity ratio, Cr I 428.9 nm/He I 438.8 nm, was observed, as presented in Fig. 2(a). The behavior of the QMB signal (red squares in Fig. 2(a)) was consistent with the spectroscopic data. The time-integrated Y was measured to be ~2.4e-2, which is very close to ~3.7e-2 from Ref. [1]. The sample surface did not turn dark after the plasma exposure (see the inset of Fig. 2(b)). SEM observations revealed that cone structures did not form on the surface, except at isolated spots, as demonstrated in Fig. 2(b). Similarly, Ne plasma exposure did not lead to the cone structure formation, and the sputtering yield was consistent with Ref. [1].

3.3. NAGDIS-II

A further comparison was made in NAGDIS-II. Fig. 3(a) shows the time evolution of an intensity ratio, Cr I 425.4 nm/He I 438.8 nm, during He plasma exposure. It was observed that the intensity ratio decreased by a factor of ~2.5. The time-integrated Y was around 6.5e-3, which is higher than that in PISCES-A, but is lower than the theoretical value of ~3.7e-2. On the surface, cone structures formed non-uniformly as seen in Fig. 3(b). The size and density of the cones look different from those in PISCES-A. This may explain the higher Y measured in NAGDIS-II than that measured in PISCES-A.

4. Discussion

First, we discuss the cause of the apparently inconsistent experimental results between the three devices, which in turn can explain the cause of the cone structure formation. Later, further mechanisms for the cone structure formation are discussed.

4.1. Influence of heavier impurity deposition

The most plausible cause is thought to be related to the different sample holding systems in each device, as shown in Fig. 4. A Cr sample with the diameter of 25 mm was clamped with a Ta cap onto the sample manipulator in PISCES-A, as presented in Fig. 4(a). The front surface shape of the Ta cap is hexagonal with the long diagonal of 38 mm, and the cap has an opening hole with the diameter of 22 mm at the center

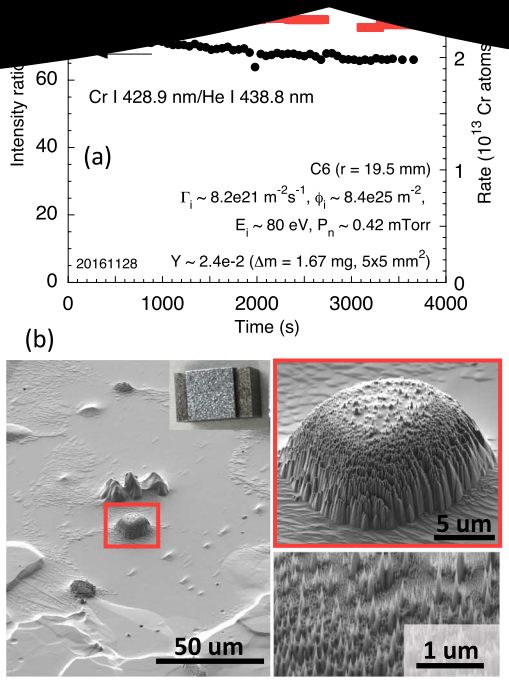

Fig. 2. Typical Cr sputtering experimental result in PSI-2. (a) Time evolution of the intensity ratio, Cr I 428.9 nm/He I 438.8 nm, measured in front of a Cr sample during He plasma exposure. (b) SEM images of the Cr sample after the He plasma exposure at different magnifications (an enlarged image of the area enclosed with the red square on the left is shown on the top right). A photo of the entire Cr sample is shown in the inset.

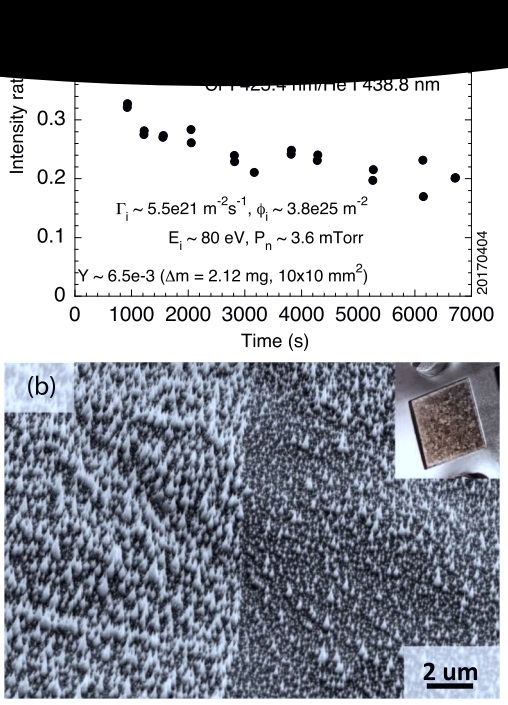

Fig. 3. Typical Cr sputtering experimental result in NAGDIS-II. (a) Time evolution of the intensity ratio, Cr I 425.4 nm/He I 438.8 nm, measured in front of a Cr sample during He plasma exposure. (b) SEM image of the Cr sample after the He plasma exposure. A photo of the entire Cr sample is shown in the inset.

for the plasma exposure to the Cr sample. Since the diameter of the plasma column is around 50 mm, both the Cr sample and the Ta cap were simultaneously exposed to the plasma. In NAGDIS-II (see Fig. 4(c)), a Mo cover was used to hold a Cr sample with a square shape (the exposure area of the sample: 10×10 mm^2). Thus, similarly to PISCES-A, both the Cr sample and the Mo cover were simultaneously exposed to the plasma with the diameter of ~25 mm. In contrast, the plasma contacted only Cr in PSI-2, as seen in Fig. 4(b). Ten Cr samples with the exposed area of 5×5 mm^2 of each sample were held with a Cr plate (100×80 mm^2) larger than the diameter of the plasma column. Note that, four Mo bolts were used to fix the Cr plate onto the back plate attached to the sample manipulator, and might have been slightly exposed to the edge low-flux plasma. The higher Cr I/He I line intensity ratio in PSI-2, as presented in Fig. 2(a), is due partly to the larger exposed surface area of Cr.

The sputtering yield of Mo (< 1e-3) and Ta by He at $E_i \sim 80$ eV is much lower than that of Cr [1]. In particular, the threshold energy of Ta sputtering by He is higher than 100 eV. Initially, we ruled out the influence of Mo and Ta sputtering and subsequent deposition on the cone formation. However, a small amount of Ta (~2 at%) was detected on a Cr sample exposed to a He plasma in PISCES-A with EDX (energy-dispersive X-ray spectroscopy) analysis at a low electron energy of 5 kV. AES (Auger electron spectroscopy) analysis, which is more sensitive to the surface, also detected Ta. Furthermore, in-situ LIBS (laser-induced breakdown spectroscopy) measurements during He plasma exposure in PISCES-A detected Ta on the surface of a Cr sample, only after cone structures developed [10]. Based on these surface analyses, it is speculated that Ta (or Mo in NAGDIS-II) is sputtered by a trace amount of intrinsic impurities (C, O, etc) ions as well as Cr ions, originated from sputtering of the Cr target. Subsequently, sputtered Ta (or Mo) atoms can deposit on the Cr surface. Deposited Ta (or Mo) atoms can then agglomerate on the Cr surface, and can act as a point source of a cone, since the sputtering yield of Ta (or Mo) is much lower than that of Cr, as mentioned above. As cones grow, the sputtering yield of Cr decreases, as observed with spectroscopy, due to the line-of-sight redeposition of sputtered Cr atoms onto the neighboring cones.

A higher concentration of Ta at the tip of cones was observed on a Be sample exposed to D + He (~10% He^+) mixture plasma at $E_i \sim 100$ eV in PISCES-B. Note that the sample holding system in PISCES-B is the same as in PISCES-A, and a Ta cap was used to clamp the Be sample. The Be sample was thinned with the FIB (focused ion beam) technique for cross-sectional observations after the plasma exposure. Fig. 5(a) shows a HAADF-STEM (high-angle annular dark-field scanning transmission electron microscopy) image of a cross-section of the Be sample with cones. Since high-Z atoms are observed to be brighter in a HAADF-STEM image, it appears that high-Z atoms exist at the tip of cones. Furthermore, EDX analysis presented in Fig. 5(b) reveals that the high-Z atoms at the tip of cones is Ta. While the lower part of cones also looks bright in both the images, this is considered to be due to the more overlapping of cones at the lower part along the line of sight. Apart from this artificial effect, it seems that Ta atoms do not perfectly nucleate at the tip of cones, but somewhat decorate the cones.

In PISCES-A, two additional experiments were conducted without a much heavier material simultaneously exposed to plasma. Namely, a Cr sample larger than the plasma column was exposed in the first experiment, and the second experiment used a stainless steel (the main components are Fe, Cr, and Ni) cap with the same dimension as the Ta one. The first experiment is a duplicate of the experiment in PSI-2. As expected, a Cr I 425.4 nm/He I 447.1 nm line intensity ratio did not show a significant decay during He plasma exposure (see Fig. 6(a)). Similarly, the stainless steel cap did not lead to a decay of the intensity ratio during He plasma exposure, as presented in Fig. 6(b). Note that, since it was hard to keep T_s low with the stainless steel cap, the plasma

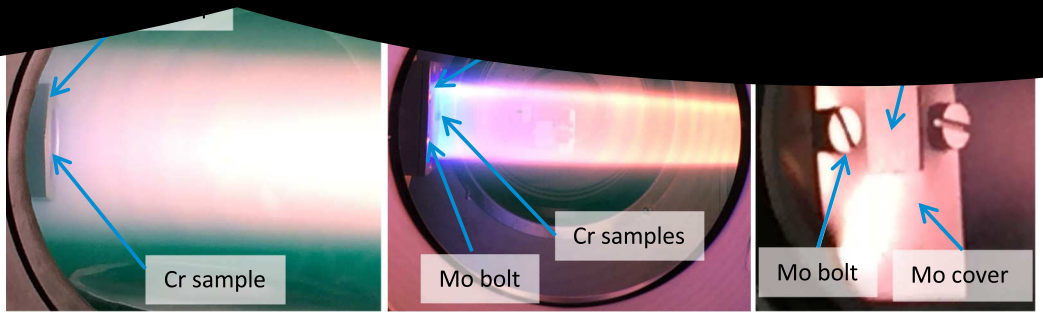

Fig. 4. Sample holding configurations in (a) PISCES-A with a Ta cap, (b) PSI-2 with a Cr plate and Mo bolts, and (c) NAGDIS-II with a Mo cover and Mo bolts.

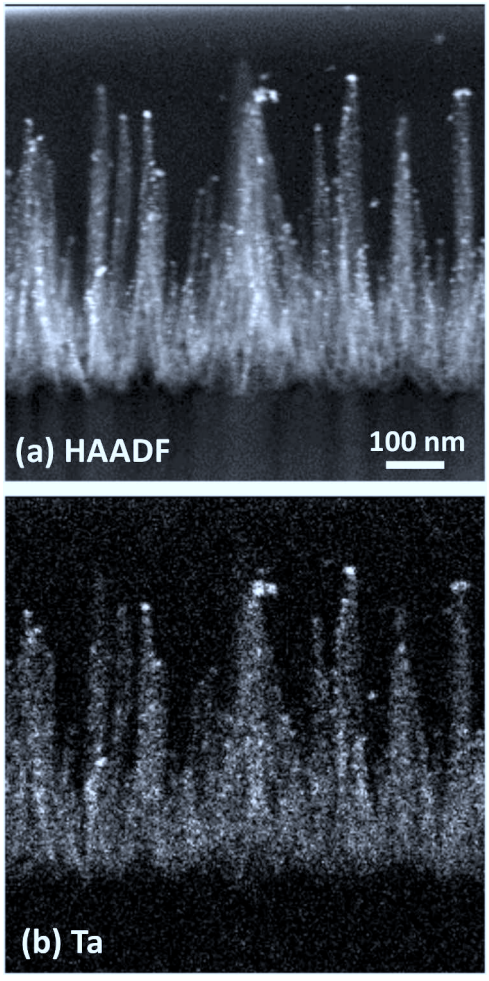

Fig. 5. (a) HAADF-STEM image of the surface of a Be sample after D + He (~10% He^+) mixture plasma exposure at E_i ~ 100 eV. (b) EDX mapping of Ta.

exposures to the Cr sample were interrupted at a short duration (~600 s) with a dump plate located in front of the sample. While the cause for the slight increase in the intensity ratio is not clear, it may be related to the increased erosion of Cr from the stainless steel cap due to the temperature increase, as the cap temperature may be higher than the sample temperature T_s. As a consequence, Y was measured to be around 4.4e-2 for the first experiment and 3.5e-2 for the second one, both of which are very similar to the theoretical value of ~3.7e-2. These experiments further confirm the influence of heavier impurity deposition on the cone formation.

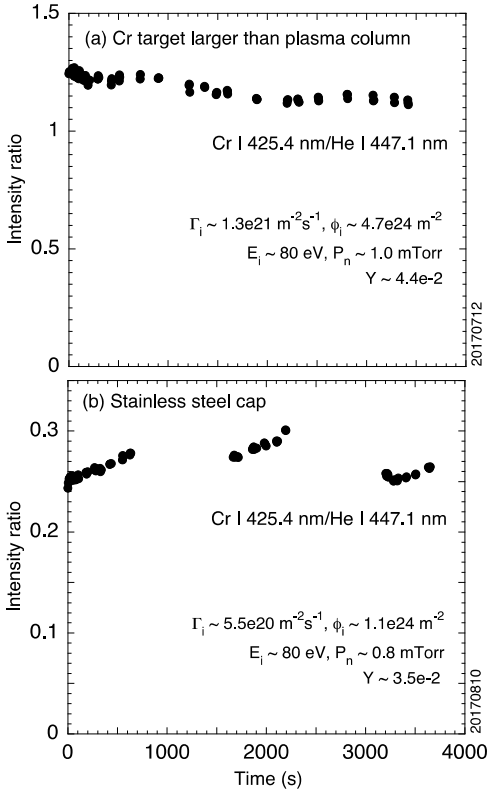

Fig. 6. Time evolution of the intensity ratio, Cr I 425.4 nm/He I 447.1 nm, during He plasma exposure to (a) a Cr sample larger than the plasma column and (b) a Cr sample with a stainless steel cap in PISCES-A.

It should be noted that our experimental observations are basically consistent with a recently published study [11], where Fe and Cu targets were exposed to D plasma at E_i ~ 140 and 200 eV with and without W impurity seeding. With W seeding, nano-sized structures were observed, and hence the sputtering yield of Fe and Cu was reduced.

As mentioned above, Ne plasma exposure did not lead to the formation of cone structures even with a Ta cap in PISCES-A, which is consistent with our previous experiments using other metals [2–4]. The Ta cap is sputtered by Ne, and sputtered Ta atoms can redeposit on the Cr surface. However, cone structures do not develop, because the redeposited Ta atoms can be easily re-sputtered by Ne.

4.2. *Other possible mechanisms*

In PSI-2, cones were observed only in isolated spots, as presented in

D or He p
ap in PISCES-B [3]. This means that th
exist other mechanism(s) to induce cone structures other than heavier impurity deposition. Here, we discuss effects of surface irregularity and oxide.

As discussed in Ref. [3], surface irregularity [12] may be responsible for the formation of cone structures without heavier impurities. In this mechanism, the incident angle dependence of sputtering yield plays an important role in forming cones. Oxide on the surface may also lead to cone structures, because the sputtering yield of oxides is lower than that of pure metals. For instance, the sputtering yield of BeO is a few times lower than that of Be [13]. Although our previous work showed that most or all of the initially existent oxygen was removed from a Be surface at the beginning of He plasma exposure [14], a trace amount of intrinsic oxygen in the plasma may continuously form an oxide on the surface, which is in competition with sputtering. It should be noted that, as the density of cones without heavier impurities has been observed to be lower than that with heavier impurities, it can be said that heavier impurity deposition is the dominant mechanism, and speeds up the formation of cone structures.

As briefly mentioned in Section 1, the following mechanism may also need to be considered for the sputtering yield reduction. A high gas density, or so called saturation, layer in the near surface can be built up due to high-flux low-energy plasma exposure. According to Ref. [15], a high D concentration of ~10 at% within 10 nm from the surface of a W sample was measured using a post-mortem analysis technique. This indicates that the D concentration in the near surface during plasma exposure is even higher than 10 at%, since dynamic retention of gas atoms quickly decays after plasma exposure [10,16,17]. Such a saturation layer with a high gas density can have two effects on sputtering: (1) simply lower the lattice atom density, and (2) act to shield the lattice atoms from the incoming particle momentum [4], both of which can lead to the reduction of the sputtering yield. The effects of a saturation layer on sputtering discussed above still need to be verified.

5. Conclusion

Collaborative experiments between three linear plasma devices (PISCES-A, PSI-2, and NAGDIS-II) were conducted to investigate the development of surface morphology on, and the resultant reduction of sputtering yield of, Cr as a test material due to light ion (He in the experiments presented here) plasma exposure. It was identified that heavier impurity (Mo or Ta here) deposition on the surface is the major factor to facilitate the formation of cone structures. Be experiments in PISCES-B showed the formation of cone structures even without heavier impurity deposition, but the density of cones was lower than with
field may
nal conductivity of cones may be lower than that of the bulk. Effect of cone structures on arc ignition will be studied in the future.

In ITER with Be and W as plasma-facing materials, cone structures may form on the surface of Be tiles as a result of W sputtering, migration, and deposition onto Be. Since it is expected that radiator gases such as Ne and Ar will be injected into the plasma to enhance radiation loss, the growth of cone structures can be hindered.

Declaration of Interest

None.

Acknowledgements

This work is supported by the US DOE Grant: DE-FG02-07ER54912, and is conducted as part of IEA Technology Collaboration Programme on the Development and Research on Plasma Wall Interaction Facilities for Fusion Reactors.

References

[1] W. Eckstein, Sputtering yields, in: R. Behrisch, W. Eckstein (Eds.), Sputtering by Particle Bombardment, Springer-Verlag, Berlin, 2007, p. 33.
[2] R.P. Doerner, D. Nishijima, T. Schwarz-Selinger, Phys. Scr. T159 (2014) 014040.
[3] R.P. Doerner, M.J. Baldwin, D. Nishijima, J. Nucl. Mater. 455 (2014) 1.
[4] R.P. Doerner, Scripta Materialia 143 (2018) 137.
[5] D. Nishijima, M.J. Baldwin, R.P. Doerner, J.H. Yu, J. Nucl. Mater. 415 (2011) S96.
[6] S. Kajita, T. Yoshida, D. Kitaoka, R. Etoh, M. Yajima, et al., J. Appl. Phys. 113 (2013) 134301.
[7] D.M. Goebel, G. Campbell, R.W. Conn, J. Nucl. Mater. 121 (1984) 277.
[8] A. Kreter, C. Brandt, A. Huber, S. Kraus, S. Moller, et al., Fusion Sci. Technol. 68 (2015) 8.
[9] N. Ohno, D. Nishijima, S. Takamura, Y. Uesugi, M. Motoyama, et al., Nucl. Fusion 41 (2001) 1055.
[10] D. Nishijima, M. Patino, R.P. Doerner, Review of Scientific Instruments 89 (2018) 10J105.
[11] V.Kh. Alimov, Y. Hatano, M. Balden, M. Oyaizu, K. Isobe, et al., Nucl. Mater. Energy 13 (2017) 81.
[12] B.I. Prenitzer, C.A. Urbanik-Shannon, L.A. Giannuzzi, S.R. Brown, R.B. Irwin, et al., Microsc. Microanal 9 (2003) 216.
[13] J. Roth, W. Eckstein, M. Guseva, Fusion Eng. Des. 37 (1997) 465.
[14] R.P. Doerner, C. Björkas, D. Nishijima, T. Schwarz-Selinger, J. Nucl. Mater. 438 (2013) S272.
[15] L. Gao, W. Jacob, U. von Toussaint, A. Manhard, M. Balden, et al., Nucl. Fusion 57 (2017) 016026.
[16] V. Philipps, J. Ehrenberg, J. Vac. Sci. Technol A 11 (1993) 437.
[17] S. Möller, D. Matveev, Y. Martynova, B. Unterberg, M. Rasinski, et al., Nucl. Fusion 57 (2017) 016020.